



# Airborne in situ vertical profiling of HDO / H<sub>2</sub><sup>16</sup>O in the subtropical troposphere during the MUSICA remote sensing validation campaign

C. Dyroff<sup>1</sup>, S. Sanati<sup>1</sup>, E. Christner<sup>1</sup>, A. Zahn<sup>1</sup>, M. Balzer<sup>2</sup>, H. Bouquet<sup>2</sup>, J. B. McManus<sup>3</sup>, Y. González-Ramos<sup>4</sup>, and M. Schneider<sup>1</sup>

<sup>1</sup>Karlsruhe Institute of Technology (KIT), Institute of Meteorology and Climate Research (IMK-ASF), Karlsruhe, Germany

<sup>2</sup>Karlsruhe Institute of Technology (KIT), Institute for Data Processing and Electronics (IPE), Karlsruhe, Germany

<sup>3</sup>Aerodyne Research Inc., 45 Manning Road, Billerica, MA 01821, USA

<sup>4</sup>Agencia Estatal de Meteorología (AEMET), Santa Cruz de Tenerife, Spain

Correspondence to: C. Dyroff (christoph.dyroff@kit.edu)

Received: 2 December 2014 – Published in Atmos. Meas. Tech. Discuss.: 6 January 2015

Revised: 7 April 2015 – Accepted: 13 April 2015 – Published: 9 May 2015

**Abstract.** Vertical profiles of water vapor (H<sub>2</sub>O) and its isotope ratio D/H expressed as  $\delta D(H_2O)$  were measured in situ by the ISOWAT II diode-laser spectrometer during the Multi-platform remote Sensing of Isotopologues for investigating the Cycle of Atmospheric water (MUSICA) airborne campaign. We present recent modifications of the instrument design. The instrument calibration on the ground as well as in flight is described. Based on the calibration measurements, the humidity-dependent uncertainty of our airborne data is determined. For the majority of the airborne data we achieved an accuracy (uncertainty of the mean) of  $\Delta(\delta D) \approx 10\%$ . Vertical profiles between 150 and  $\sim 7000$  m were obtained during 7 days in July and August 2013 over the subtropical North Atlantic Ocean near Tenerife. The flights were coordinated with ground-based (Network for the Detection of Atmospheric Composition Change, NDACC) and space-based (Infrared Atmospheric Sounding Interferometer, IASI) FTIR remote sensing measurements of  $\delta D(H_2O)$  as a means to validate the remote sensing humidity and  $\delta D(H_2O)$  data products. The results of the validation are presented in detail in a separate paper (Schneider et al., 2014). The profiles were obtained with a high vertical resolution of around 3 m. By analyzing humidity and  $\delta D(H_2O)$  correlations we were able to identify different layers of air masses with specific isotopic signatures. The results are discussed.

## 1 Introduction

The stable isotopologues of atmospheric water (H<sub>2</sub>O) vapor contain information about its condensation history, because the isotopologue ratios are altered whenever H<sub>2</sub>O is subjected to phase changes (Dansgaard, 1964). Evaporation and condensation leave a fingerprint in the isotopologue ratios due to differences in vapor pressure and kinetic diffusion properties of the isotopologues (Dansgaard, 1964; Merlivat, 1978; Jouzel and Merlivat, 1984). This fingerprint is mainly depending on temperature (vapor pressure), but it also contains information of relative humidity (kinetic effect) during evaporation. Mixing of different air masses induces further changes of the isotopic composition of air masses probed (Noone et al., 2011).

In this paper we discuss changes in the ratio  $R_D = D/H$  in water vapor, which are expressed with respect to the Vienna Standard Mean Ocean Water (VSMOW) reference standard as  $\delta D(H_2O) = R_{D(\text{Sample})}/R_{D(\text{VSMOW})} - 1$  (typically given in ‰).

On a global scale, remote sensing measurements of  $\delta D(H_2O)$ , abbreviated herein as  $\delta D$ , can help to better constrain the condensation history and transport pathways from the ground to the sampling location. Tropospheric profile measurements have already been reported from ground and space by means of Fourier Transform Infrared (FTIR) spectroscopy or other techniques (Kuang et al., 2003; Zakharov et al., 2004; Worden et al., 2006; Frankenberg et al., 2009;

Risi et al., 2010; Randel et al., 2012; Risi et al., 2012; Schneider et al., 2012). Since changes of  $\delta D$  are usually small, uncertainties in its determination (accuracy) may lead to misinterpretation of the physical processes involved in the H<sub>2</sub>O transport.

Quality assessment of remotely sensed  $\delta D$  has been performed theoretically (Worden et al., 2006; Schneider et al., 2006; Schneider and Hase, 2011; Lacour et al., 2012; Schneider et al., 2012; Boesch et al., 2013). So far empirical validation studies of tropospheric  $\delta D$  remote sensing products have been made with very few indirect references (Worden et al., 2011) or have used a  $\delta D$  reference that itself was not comprehensively validated (Schneider and Hase, 2011; Boesch et al., 2013). Recently Herman et al. (2014) presented reference data for space-based remote sensing observations of the Tropospheric Emission Spectrometer (TES), which is important progress. However, their profile measurements were limited to the lower  $\sim 4500$  m of the troposphere and did not fully cover the altitude range of the remote sensor's peak sensitivity.

Vertical profiles of calibrated in situ  $\delta D$  measurements with well-known accuracy are highly desirable in order to prove the quality of remotely sensed  $\delta D$ . Furthermore, highly resolved in situ profiles can serve to study small-scale (tens to hundreds of meters) processes related to tropospheric humidity, e.g., cloud formation (Bolot et al., 2013) and air mass mixing (Noone et al., 2011).

In situ airborne measurements have been performed with different techniques and on various platforms (Webster and Heymsfield, 2003; Sayres et al., 2009; Iannone et al., 2009; Sodemann et al., 2013). With the exception of Herman et al. (2014), these measurements were performed without what we believe is a critical component especially for a validation experiment: inflight instrument-performance analysis by measuring a calibration-gas standard. Only if one can prove that airborne measurements of a calibration-gas standard are reproducible within the stated instrument uncertainty are these measurements an adequate source of data for remote sensing validation purposes.

In this paper we present high-resolution tropospheric vertical profiles of  $\delta D$  obtained in situ by the ISOWAT airborne tunable diode laser spectrometer during the MUlti-platform remote Sensing of Isotopologues for investigating the Cycle of Atmospheric water (MUSICA) remote sensing validation campaign. We first describe our in situ instrument which has been adapted from a previous prototype to meet the requirements for the profile measurements. We discuss our calibration procedure and derive the uncertainties of our airborne data. Then the MUSICA airborne campaign is introduced, and the vertical profiles are presented. In the last part we introduce how measurements of water isotopologues trace tropospheric transport processes.

## 2 ISOWAT II

### 2.1 Instrument setup

The ISOWAT II tunable diode laser spectrometer is based on the first prototype version (Dyroff et al., 2010), which is presently being operated onboard the IAGOS-CARIBIC passenger aircraft. ISOWAT II features a number of modifications that were implemented for the instrument operation during the MUSICA aircraft campaign. The basic instrument concept is reviewed briefly, and the modifications are discussed in the following section.

The ISOWAT instrument is a tunable diode laser absorption spectrometer to measure rotational–vibrational resolved absorption lines of the three main isotopologues of water: H<sub>2</sub><sup>16</sup>O, H<sub>2</sub><sup>18</sup>O, and HDO at a wavelength of  $\lambda = 2.65 \mu\text{m}$  ( $\nu = 3765 \text{ cm}^{-1}$ ). In the spectrometer (Fig. 1), the beam of a distributed feedback diode laser (Nanoplus GmbH) is collected by an anti-reflection coated  $f = 25.4$  mm bi-convex CaF<sub>2</sub> lens. The beam is then focused and steered into an astigmatic-type multipass absorption cell (MPC, model AMAC-76-LW, Aerodyne Research, Inc.) by means of a spherical-mirror telescope comprising a  $f = 250$  mm concave and a  $f = -100$  mm convex spherical mirror. The MPC is aligned to  $N = 110$  passes to achieve a total absorption pathlength of  $l = 36.1$  m within a volume of  $V = 0.5$  L. The beam exiting the MPC is collected and focused by a  $f = 100$  mm spherical mirror onto the thermoelectrically (TE) cooled HgCdTe sample detector (SD, model J19-TE4, Judson Technologies).

A fraction of the laser beam is picked off by a pellicle beam splitter (P-BS, 45 % / 55 %) upstream of the MPC. This beam is split again by a second P-BS and it serves two purposes. One part is guided through a 10 cm long reference-gas cell filled with a high mixing ratio of H<sub>2</sub>O. This beam is subsequently focused onto the TE-cooled InSb reference detector (RD, model J12-TE2, Judson Technologies). Spectra from the RD are used for active locking of the laser wavelength to the absorption lines of interest by applying a feedback to the laser-injection current  $I_{LD}$ . The second part of the beam is simply passing through the optical compartment of the instrument and is focused onto the TE-cooled HgCdTe background detector (BD, model J19-TE4, Judson Technologies). The BD is used to record spectra of residual water vapor present in the optical compartment. This open-path signal component is also accounted for in the SD spectra by including it in the fit. The optical paths in the SD and BD beams are closely matched.

In addition to recording the residual humidity using the BD, for ISOWAT II the optics compartment was sealed and actively dried to a relative humidity below 5 %. To this end, a miniature pump (1410 Series, Gardner Denver Thomas GmbH) constantly circulated air from the compartment (Fig. 1). This air was dried in a desiccant cartridge containing molecular sieve (0.3 nm pore width) before it was re-

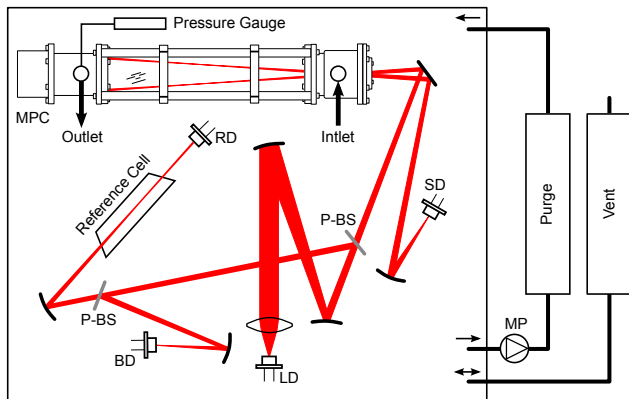


**Figure 1.** Optical system of the ISOWAT II spectrometer. LD: laser diode; P-BS: pellicle-beam splitter; MPC: multipass cell; SD: sample detector; RD: reference detector; BD: background detector; MP: miniature pump.

directed into the optics compartment. Furthermore, the optics compartment had an open port to ambient pressure (instrument surrounding) via a second desiccant cartridge. This was used as ventilation for the instrument as the aircraft cabin pressure during the campaign was varying between 1000 hPa at ground level and around 450 hPa at the highest flight level.

For ISOWAT II an entirely new digital data acquisition system has been developed. This system has two main components. A compact embedded PC (KONTRON, model pTX-SP 2.5" SBC) provides a user interface to adjust all parameters for the laser control and data acquisition. These parameters are transferred to the second component, i.e., a digital data processing unit based on field-programmable gate array (FPGA, ALTERA, model Arria GX) technology.

In ISOWAT II we employ wavelength-modulation spectroscopy (WMS) with second harmonic detection. The laser wavelength is scanned via the laser-injection current at a frequency of  $f_{\text{scan}} = 10$  Hz across four absorption lines of interest using a triangular waveform (Fig. 2). In addition, the laser wavelength is modulated with a sinusoidal waveform at a frequency of  $f_{\text{mod}} = 37.5$  kHz. All waveforms are generated by the FPGA and are converted to analog voltages using a 16 bit digital-to-analog converter.

The detector signals of SD, RD, and BD are first filtered using individual analog bandpass filters (Sallen–Key fourth-order filter,  $f_{c1} = 41$  kHz,  $f_{c2} = 121$  kHz) with  $10 \text{ dB dec}^{-1}$  efficiency. The individual signals are then amplified using computer-controlled low-noise amplifiers in order to utilize the full range of the 16 bit analog-to-digital converters (ADC). After digitization, three individual software lock-in amplifiers realized in the FPGA demodulate the detector signals at  $2 \times f_{\text{mod}}$ . The demodulated signals are then fed through software low-pass finite impulse response filters with a cut-off frequency of  $f_c = 500$  Hz. The second-harmonic spectra are then transferred to the embedded PC via USB connection for storage and further processing.

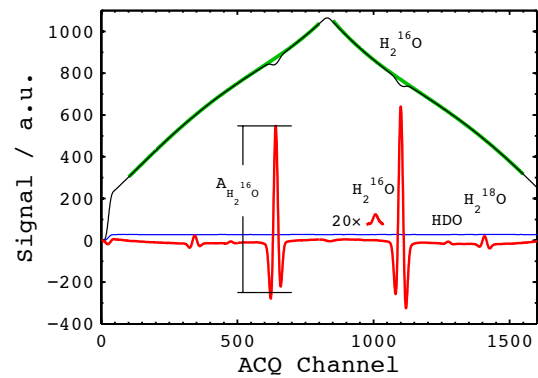


**Figure 2.** Example spectra of ISOWAT II showing the up and down scan across the absorption region of interest. Polynomial baseline (green trace) of the direct absorption spectra (black trace) as well as detector zero signal (blue trace) are used to normalize the second-harmonic absorption spectra (red trace).  $A_{\text{H}_2^{16}\text{O}}$  is the peak-to-peak amplitude of the strong  $\text{H}_2^{16}\text{O}$  absorption line. The weak  $\text{H}_2^{16}\text{O}$  line used in humid conditions is depicted 20× enlarged.

In addition to the second-harmonic spectra we record direct absorption spectra of the SD for power normalization purposes. To this end, the modulated analog SD signal used for the WMS is amplified and digitized by a 16 bit ADC. A software low-pass filter with  $f_c = 500$  Hz in the FPGA equivalent to the one used for WMS signals further conditions the signal. The spectral baseline is fit with a fourth-order polynomial (thick green line in Fig. 2). Furthermore the SD dark signal was measured every 10 min by switching off the laser diode for 10 s. The direct absorption signal was used to identify changes in the laser-power transmission through the MPC.

## 2.2 Calibration

Instrument calibration was performed using a unit for ground-based pre- and post-flight calibrations. Dry synthetic air (Air Liquide, ALPHAGAZ 1) from a compressed cylinder was humidified in a 2 L volume bubbler filled with 500 mL of a liquid isotope working standard ( $\delta\text{D} = -59.22 \pm 0.7$  ‰) at a temperature of 21 °C. This humidified air was subsequently diluted into a main flow of dry synthetic air. By adjusting the flow through the bubbler as well as the main dry air flow, the calibration humidity could be adjusted from a few hundred ppmv to more than 30 000 ppmv at  $\delta\text{D}_{\text{CAL}} \sim -137$  ‰.

The relatively large amount of liquid isotope standard used in the ground-based calibration unit was replaced daily. This was effectively reducing drift in the isotopic composition due to evaporation of the bulk water source to  $< 0.5$  ‰ in 4 h of calibration. This drift was accounted for in the data analysis. The ground-based calibration unit was independently examined prior to the campaign using a laboratory-based Picarro water isotope analyzer in combination with a standard delivery module. The repeatability was found to be better than

0.5 ‰ for  $\delta D$ , and the uncertainty in the measurement of the liquid standards was 0.7 ‰.

A dew-point hygrometer (Edge Tech, model DewMaster) was occasionally connected in parallel to ISOWAT on the ground in order to perform absolute humidity measurements that served as calibration of the H<sub>2</sub><sup>16</sup>O and HDO absorption-line fit.

Similar to the first version of ISOWAT (Dyroff et al., 2010), during MUSICA the instrument was equipped with a calibration-gas source for inflight instrument-performance analysis. To provide a calibration-gas mixture of known isotopic composition, a flow of 3.5 slpm (1 slpm = 1000 cm<sup>3</sup> air at 1000 hPa) of ambient air was first dried to H<sub>2</sub>O < 5 ppmv in a desiccant cartridge containing molecular sieve (0.3 nm pore width). A part (0.1 slpm) of this dry air flow was humidified by passing it through a small temperature-controlled bubbler ( $T = 45 \pm 0.05$  °C) that contained a liquid-water isotope-working standard ( $\delta D = -59.22 \pm 0.7$  ‰). The well-known fractionation factor for evaporation of the liquid water standard is  $\alpha(T = 45$  °C)  $\sim 1.06$ , which leads to water vapor with  $\delta D \sim -116$  ‰. The pressure in the bubbler thereby corresponded to the ambient air pressure. The humidified flow was then mixed into the main dry air flow to produce a calibration gas with a (pressure-dependent) humidity of around 3000 and 5000 ppmv at ground level and 6000 m flight altitude. The inflight calibration-gas source was cross-calibrated by three measurements before and after each flight using this primary standard.

The calibration gas was fed into ISOWAT II two to five times per flight in a variety of situations, including relatively rapid ascends or descends and high turbulence at lower flight levels in order to ensure instrument performance in these conditions. The MPC was first flushed with the calibration gas for 7 min to allow for complete isotope exchange. Then a calibration-gas spectrum was recorded for 2 min, after which the MPC was flushed with ambient air for 7 min before continuation of ambient-air measurements.

### 2.3 Data handling

Ten second-harmonic ( $2f$ ) spectra are averaged in 1 s and normalized by optical power at the sample detector ( $P_{LD}$ ). We therefore use the spectral baseline of the simultaneously recorded direct absorption channel together with the detector zero signal. The latter is linearly interpolated between measurements taken every 10 min where the laser was switched off for 10 s. The normalized  $2f$  spectra are then divided into windows around the individual absorption lines.

For the strong H<sub>2</sub><sup>16</sup>O line we determine the peak-to-peak amplitude  $A_{H_2^{16}O}$  based on the signal at line center and the minima of the two negative lobes of the  $2f$  absorption line. This is then compared to  $A_{H_2^{16}O}$  from a previously recorded calibration spectrum in order to derive the H<sub>2</sub>O mixing ratio. The shape and amplitude of the strong H<sub>2</sub><sup>16</sup>O line are con-

siderably affected by absorption-line self-broadening (Burch et al., 1962).

The other absorption lines are much less affected by line broadening, and in each fit window a linear least squares fit is performed using singular value decomposition (SVD) (Dyroff et al., 2010). The SVD fit includes constant and linear baseline terms, as well as the line component from the calibration spectrum, and it yields the mixing ratio of the individual isotopologues. From the mixing ratios the isotopologue ratios are determined.

First we transferred the peak-to-peak absorption-line signal  $A_{H_2^{16}O}$  onto a humidity scale based on the humidity calibrations performed using the dew-point hygrometer. Then we determined the humidity-dependent correction functions  $CF(H_2O)$  for the raw isotopologue ratio  $R_D^* = HDO/H_2^{16}O$  as depicted in Fig. 3a. For the  $CF(H_2O)$  of the strong H<sub>2</sub><sup>16</sup>O line we use an empirical sixth-order polynomial and for the  $CF(H_2O)$  of the weak line a first-order polynomial (black traces in Fig. 3).

In order to transfer the raw  $R_D^*$  to  $\delta D$  on the VSMOW scale, we first divide the individual  $R_D^*$  measurements by the daily average  $CF(H_2O)$ . We then multiply by the isotopologue ratio of the calibration gas  $R_{CAL} = R_{VSMOW}(\delta D_{CAL} + 1)$ , where  $R_{VSMOW} = 3.10693 \times 10^{-4}$ , and obtain  $\delta D$  by solving

$$\delta D = \frac{R_D^*}{CF(H_2O)} R_{VSMOW} (\delta D_{CAL} + 1) - 1. \quad (1)$$

Figure 3b depicts this procedure for the calibration measurements of 25 July 2013. The black dashed lines indicate the uncertainty range, which is defined as the range of data in which  $1\sigma$  of the data fall.

Note that we have defined a transition interval between 10 000 and 12 000 ppmv in which we make use of both the strong and the weak H<sub>2</sub><sup>16</sup>O absorption line. In this interval, the individual fit results are used in a humidity-weighted manner in order to achieve a smooth transition between the two fit regimes.

### 2.4 Uncertainty estimate

The uncertainty of our  $\delta D$  measurements was derived from the calibration measurements that were performed on every flight day before and after each flight as described in Sect. 2.2. We define the uncertainty as the standard deviation of all daily calibrations to the daily mean humidity correction function for a given humidity interval  $h$ :

$$\Delta(\delta D)_h = \sqrt{\left[ \frac{1}{n-1} \sum_{i=1}^n (\delta D_i - \delta D_{CAL})^2 \right]_h}. \quad (2)$$

The uncertainty was determined in humidity intervals ( $h$ ) of 10 ppmv between 100 and 25 000 ppmv, and it is depicted for all flight days as black traces in Fig. 4.

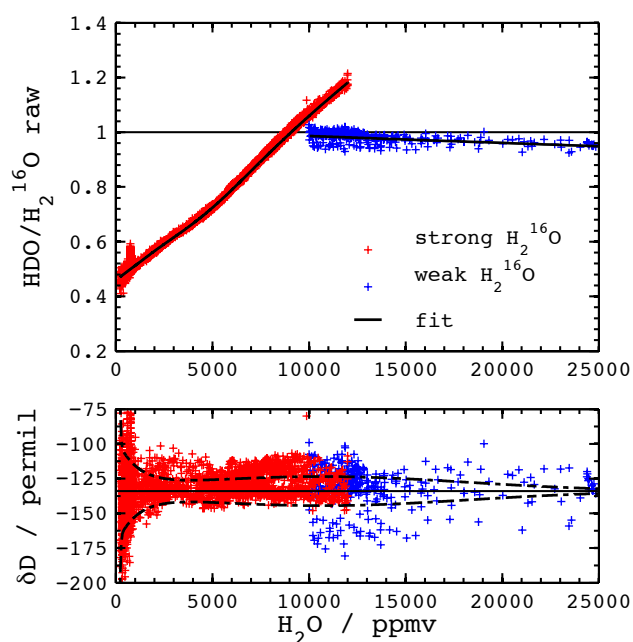


**Figure 3.** (a) Individual calibration measurements on 25 July 2013 pre- and post-flight together with the daily average calibration functions for strong (red) and weak (blue) H<sub>2</sub><sup>16</sup>O line fit. (b) Calibration measurements on VSMOW scale corrected for nonlinear response. Dashed lines indicate the 1σ confidence band.

Any differences in the instrument response before and after the flight was assigned to instrumental drift. Even though the instrument temperature was greatly stabilized, the drift was most likely caused by changes in the temperature of components that are not well temperature-stabilized (see Sect. 2.5 for detailed discussion).

In addition we have used the inflight calibration-gas measurements to verify that our uncertainty estimate was justified. The difference of these calibration measurements to the expected δD of the inflight calibration-gas standard is depicted as blue diamonds in Fig. 4. These differences are generally better or equal to the uncertainty estimation. We are thus confident that the instrumental uncertainty of our flight measurements is equal to or better than the stated uncertainty estimate.

## 2.5 Sources of uncertainty

We have identified two main factors that define the measurement uncertainty of ISOWAT II. Their importance varies throughout the investigated humidity range.

At humidities below ~1000 ppmv, optical interference fringes superimposed onto the measured absorption spectra become relevant as the measured absorption signal becomes weak. The fringes in our system during the MUSICA campaign were with OD ~ 1...2 × 10<sup>-4</sup> about 1.5–3 times higher than currently in ISOWAT-I (Dyroff et al., 2010), and their free spectral range were such that they could not easily be

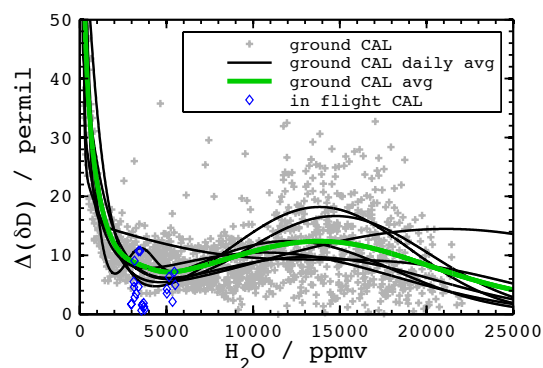


**Figure 4.** Uncertainty analysis for all flight days. Grey symbols: deviation of individual 1 Hz calibration measurements from calibration standard; black lines: daily fit of Δ(δD) (Eq. 2); green line: campaign average of Δ(δD). Inflight calibration-gas measurements are depicted as the difference to the daily mean (absolute value) by the blue symbols.

distinguished from the absorption lines by our absorption-line fit. The phase of the fringes was also changing due to slight changes in instrument temperature, which prohibited the recording of the fringes once for later subtraction while sampling dry air (background spectrum). The fringes affected mostly the HDO line at dry conditions as well as the weak H<sub>2</sub><sup>16</sup>O line below 15 000 ppmv. For example, the fractional absorption of HDO at 200 ppmv and δD = -400‰ is around 4.2 × 10<sup>-4</sup>, i.e., a signal to fringe ratio of ~2–4. The fringe amplitude can be translated to an absorption signal equivalent to around 1 ppmv (strong H<sub>2</sub><sup>16</sup>O line).

An array of residual spectra is depicted in the lower panel of Fig. 5. By repeatedly modulating the temperature of the anti-reflection coated  $f = 25.4$  mm CaF<sub>2</sub> collection lens (top panel in Fig. 5) we were able to identify this lens as the source of the most dominant fringe. The fringe free-spectral range (FSR) is estimated to be around 3.75 GHz, which translates into an optical resonator length of around 2.8 cm assuming the refractive index of CaF<sub>2</sub> of 1.43. The center thickness of the lens is 11 mm. We conclude that multiple internal reflections at a thinner part of the lens caused the fringe.

In a laboratory test after the campaign, replacement of this lens by a reflective mirror objective has reduced the overall fringe level by a factor of 2. Importantly, the FSR has become shorter by a factor of 3 to 4. This will potentially make fitting of the fringe structure easier for future measurements. We plan to carefully re-design the optical setup of ISOWAT based on the results using the mirror objective.

The second factor affecting the instrumental uncertainty was related to slight changes in the temperature of the laser-gain medium. In the present instrument, this temperature is set to a constant value (~28 °C). Then the laser emission wavelength ( $\lambda_{LD}$ ) is tuned by sweeping the laser-injection current ( $I_{LD}$ ). Despite setting  $T_{LD}$  to a constant value,  $T_{LD}$  was drifting during instrument operation. We actively con-

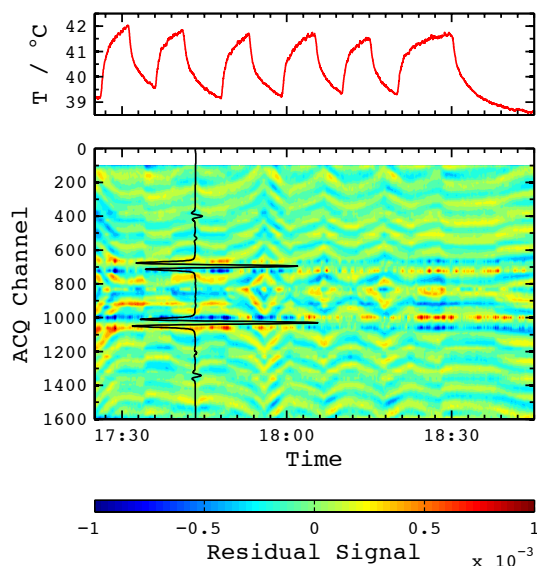


**Figure 5.** (a) Temperature recording of the mount of the  $f = 25.4$  mm collection lens. (b) Array of spectral residuals recorded in the laboratory while repeatedly modulating the temperature of the  $f = 25.4$  mm collection lens. The color code represents the residual amplitude scaled to optical density. The black trace depicts a second-harmonic spectrum recorded at 1 s integration time.

trol the DC component of  $I_{LD}$  in order to maintain the wavelength scan in the spectral window around the absorption lines of interest (line lock). Adjusting the DC component of  $I_{LD}$  changes the operating point of the laser. This affects the nonlinear response of laser power ( $P_{LD}$ ) and  $\lambda_{LD}$  to a sweep of  $I_{LD}$ . Changes in  $P_{LD}$  are accounted for by normalizing the second-derivative spectra by the direct-absorption spectra. Changes in the wavelength tuning of the laser lead to a distortion of the recorded spectra. As we determine mixing ratios and  $\delta D$  by fitting of ambient spectra to a previously recorded calibration spectrum, this distortion of the spectra adds uncertainty to the fit.

It was found after the campaign that the major source of temperature drift was a temperature-dependent potentiometer ( $100 \text{ ppm K}^{-1}$ ) on the commercial laser-driver unit. The resistance of this potentiometer changes due to changes in ambient temperature, which in turn changes the temperature set point of the laser-temperature control loop. Replacing this potentiometer with a fixed resistor with low-temperature coefficient ( $2 \text{ ppm K}^{-1}$ ) will minimize the change of the temperature set point.

Meanwhile, we have developed an improved stabilization of the laser-operating point by implementing a second control loop. In this approach we additionally control the temperature of the aluminum mount of the laser diode using resistive heaters. The temperature of the mount is adjusted such that  $\lambda_{LD}$  is maintained stable, which is determined by analyzing the position of the absorption lines within the reference-detector spectra. This in turn allows us to maintain the DC

component of  $I_{LD}$  constant. Consequently the laser operating point is stabilized. First tests in the laboratory have shown that this approach minimizes the drift of the laser-temperature set point by a factor of 11 even when using the temperature-sensitive potentiometer.

### 3 MUSICA aircraft campaign

#### 3.1 Objective and realization

The primary goal of the MUSICA airborne campaign was to perform validation measurements for two remote sensing instruments: (i) the satellite-borne Infrared Atmospheric Sounding Interferometer (IASI) instrument on both the MetOp-A and B satellites and (ii) a ground-based FTIR spectrometer at the Izaña meteorological observatory (IZO). The second goal was to investigate transport and processing of water vapor in the North Atlantic free troposphere (FT).

Seven research flights were conducted from Las Palmas Airport (LPA), Canary Islands, Spain. The Canary Islands are located in the subtropical North Atlantic, approximately 200 km west off the coast of Morocco at  $28^\circ \text{N}$  latitude (Fig. 6). The flights were coordinated in time and location with the morning overpasses of the MetOp-A and B polar-orbiting satellites (Klaes et al., 2007). Both satellites are equipped with an IASI instrument as scientific payload (Blumstein et al., 2004). IASI measures nadir radiance spectra from which tropospheric H<sub>2</sub><sup>16</sup>O, HDO, and  $\delta D$  vertical profiles are retrieved (Schneider and Hase, 2011). MetOp overpasses took place on a trajectory from northeast to southwest, where IASI scanned transversal to its flight direction. The individual spectra were filtered based on data quality and cloudiness as described in Wiegeler et al. (2014). The ground location of all quality-filtered vertical profile measurements obtained during the campaign is depicted as circles in Fig. 6.

The aircraft flights were performed in the line of sight of the ground-based FTIR instrument stationed at IZO. The FTIR measures solar absorption spectra to retrieve vertical profiles of H<sub>2</sub><sup>16</sup>O, HDO, and  $\delta D$  in the troposphere (Schneider et al., 2012). The blue lines in Fig. 6 indicate the line of sight for the beginning and the end of the profile flight on 24 July 2013. The aircraft flight track of this day is shown in red in Fig. 6.

The flights started with a relatively fast ascent to the ceiling altitude of the aircraft ( $\sim 6800$  m). The aircraft crew then waited for the overpass of the satellites before performing a slow cascaded descent with up to 10 selected levels. The levels were held for 5 min. Each flight took around 3.5 h.

#### 3.2 Aircraft and instrumentation

For the campaign, several research instruments were mounted in a CASA C-212-200 (Fig. 7) of the Instituto Nacional de Técnica Aeroespacial (INTA). The C-212 is a medium-sized transport aircraft powered by two turbo-

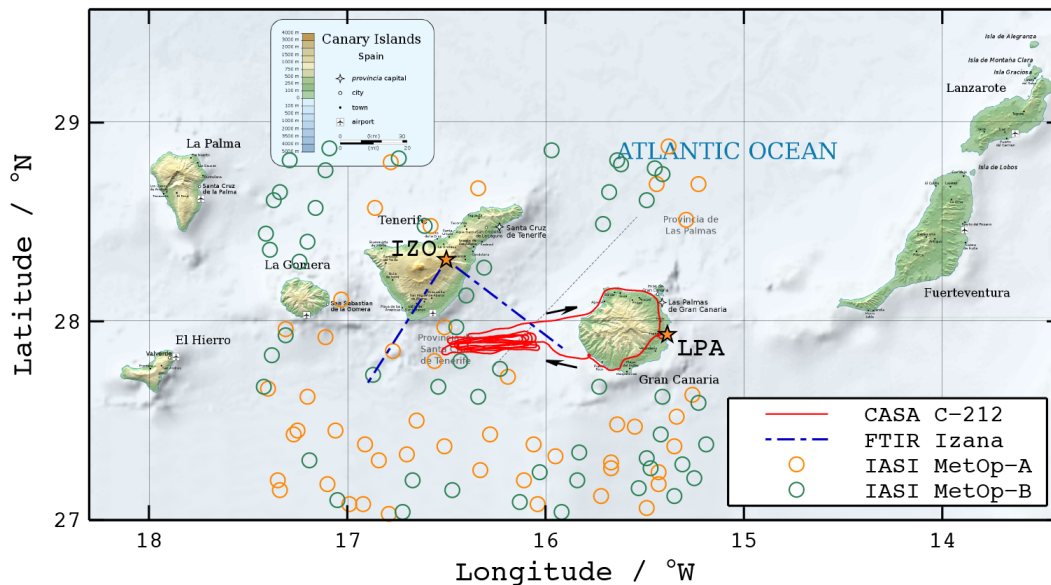


**Figure 6.** Aircraft flight track (red) of 24 July 2013 departing from Las Palmas Airport (LPA). Also shown are all MetOp-A and MetOp-B measurements (symbols) obtained during the campaign after a data-quality filter was applied. The FTIR line of sight (blue lines) for 10:30 and 13:00 UTC (start and end of profile measurements) at Izaña (IZO) is indicated. Map source: [http://en.wikipedia.org/wiki/File:Map\\_of\\_the\\_Canary\\_Islands.svg](http://en.wikipedia.org/wiki/File:Map_of_the_Canary_Islands.svg).

prop engines. It has an unpressurized cabin and can reach a maximum ceiling altitude (depending on payload) of around 23 000 ft (7000 m) with the requirement for oxygen use by the pilots and operators.

ISOWAT II was mounted in the foremost position of the aircraft cabin. Ambient air was sampled by a rearward facing stainless steel inlet with 0.25 inch (6.35 mm) outer diameter mounted on top of the aircraft fuselage (Fig. 7). A flow through the inlet line of around 15 slpm (1 slpm = 1000 cm<sup>3</sup> air at 1000 hPa) at ground level and around 6 slpm at the aircraft ceiling level was established by a membrane pump (MD1 VARIO SP, Vacuubrand GmbH) downstream of the ISOWAT II instrument. Inside the aircraft, heated ( $T = 40^{\circ}\text{C}$ ) electropolished stainless-steel tubing (ULTRON, Dockweiler AG) was used to connect the inlet system to the instrument. A flow of 1.5 slpm was branched off the main flow and fed into the ISOWAT II instrument for isotope ratio measurements. All tubes inside the instrument as well as the MPC were also heated to 40 °C.

### 3.3 Meteorological conditions

Two different meteorological conditions were encountered during the MUSICA campaign which also mark the predominant conditions at the Canary Islands in summer.

On 21 July 2013, 25 July 2013, and 30 July 2013 the marine boundary layer (MBL) was well separated from the FT by a temperature-inversion layer at an altitude of around 1100 m. This inversion is a consequence of large-scale subsidence in the downward branch of the Hadley circulation

(Cuevas et al., 2013). The subsiding air is adiabatically warmed as it reaches lower altitudes, thus yielding a well-developed temperature-inversion layer. In the MBL, winds from northeast were encountered, while in the FT the wind came from northwest. We refer to these meteorological conditions as North Atlantic owing to the air mass origin in the FT.

On 22 July 2013, 24 July 2013, 31 July 2013, and 1 August 2013 warm and mineral-dust laden air reached the Canary Islands from the east in a layer of variable thickness at an altitude of approximately 2 to 5 km. This Saharan air layer was positioned above a layer of MBL air, and it presumably originated from the African boundary layer (Rodríguez et al., 2004; Alonso-Pérez et al., 2011; Cuevas et al., 2013). We refer to these conditions as Sahara.

Figure 8 shows satellite images of the Moderate Resolution Imaging Spectroradiometer (MODIS) instrument of the days 21 July 2013 (a) and 31 July 2013 (b). In Fig. 8b one can observe the dust-laden air as the hazy area in the right half of the image. Note that the images are daily composites and may not reflect the conditions during the actual hours of flight. The flight tracks are depicted in red.

## 4 Results

Figure 9 presents an overview of the vertical profiles of H<sub>2</sub>O and  $\delta\text{D}$  as well as the estimated total uncertainty of the isotope ratio  $\Delta(\delta\text{D})$  (see Eq. 2) with a temporal resolution of 1 s. The black symbols show all inflight calibration measure-

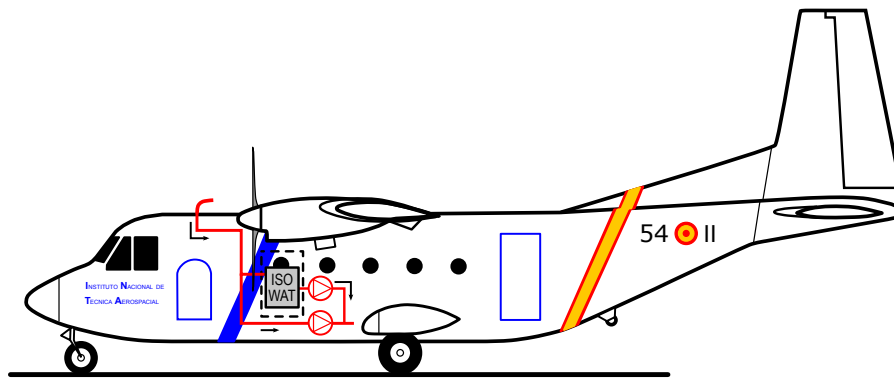


**Figure 7.** CASA C-212 aircraft of Instituto Nacional de Técnica Aeroespacial (INTA). The rear-facing ambient air inlet was located on top of the fuselage. The inlet line was flushed at a high flow using a membrane pump. ISOWAT was mounted in the foremost position of the aircraft and was equipped with a second pump to establish the gas flow through the instrument.

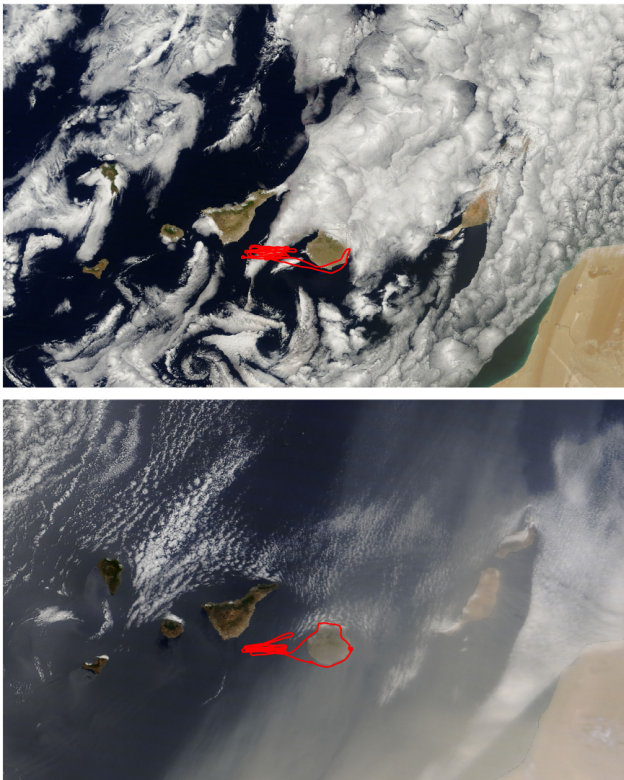


**Figure 8.** Satellite images of the Canary Islands of 21 July 2013 (top) and 31 July 2013 (bottom), which are representative of “North Atlantic” and “Sahara” conditions, respectively (for an explanation see Sect. 3.3). Images are daily composites of data of the Moderate Resolution Imaging Spectroradiometer (MODIS) aboard the NASA Terra and Aqua satellites (source: <https://earthdata.nasa.gov/labs/worldview/>). The aircraft flight tracks are depicted as red traces.

ments that were performed during the campaign. We note that the uncertainty of the inflight calibrations is in most cases smaller than  $\Delta(\delta D)$ . This provides good evidence that our uncertainty estimate can be understood as an upper limit.

For better clarity we only show in Fig. 9 the data of the descending branches of the flights. Ascent and descent took place at different times and, more importantly, at slightly different longitudes. We noticed strong longitudinal gradients in some of the flights, which prohibit averaging of the ascent and descent profiles. Good agreement of ascent and descent data is found where longitudinal gradients were low or sampling locations coincided.

For a more detailed analysis we shall have a closer look at the measurements during the descending branch of the flight on 31 July 2013. Figure 10 shows the corresponding vertical profiles of temperature ( $T$ ), H<sub>2</sub>O mixing ratio, and  $\delta D$ .

Studying the vertical profile in Fig. 10 reveals large spatial gradients in humidity and isotopic composition. We can divide the profile in five different layers.

1. The lowest layer between sea level and  $\sim 440$  m is characterized by a rather constant  $T$ , H<sub>2</sub>O, and  $\delta D$ .
2. Above this layer we observed a well-defined temperature inversion which came along with a sharp negative gradient in both H<sub>2</sub>O and  $\delta D$ . At its minimum at an altitude of  $\sim 900$  m, H<sub>2</sub>O decreased to less than 2000 ppmv (relative humidity  $\sim 8\%$ ) at  $\delta D < -300\%$ .
3. A third layer starts at  $\sim 1025$  m with a sharp positive gradient of H<sub>2</sub>O and  $\delta D$ , which is then followed by relatively constant humidity and slightly increasing  $\delta D$  until an altitude of around 1900 m.
4. The fourth and thickest layer is characterized by a column of high humidity and high  $\delta D$ , which stretches nearly 3.5 km between around 1900 m and 5350 m altitude. It is a weakly stable layer with a temperature lapse rate of  $8.6 \text{ K km}^{-1}$ .

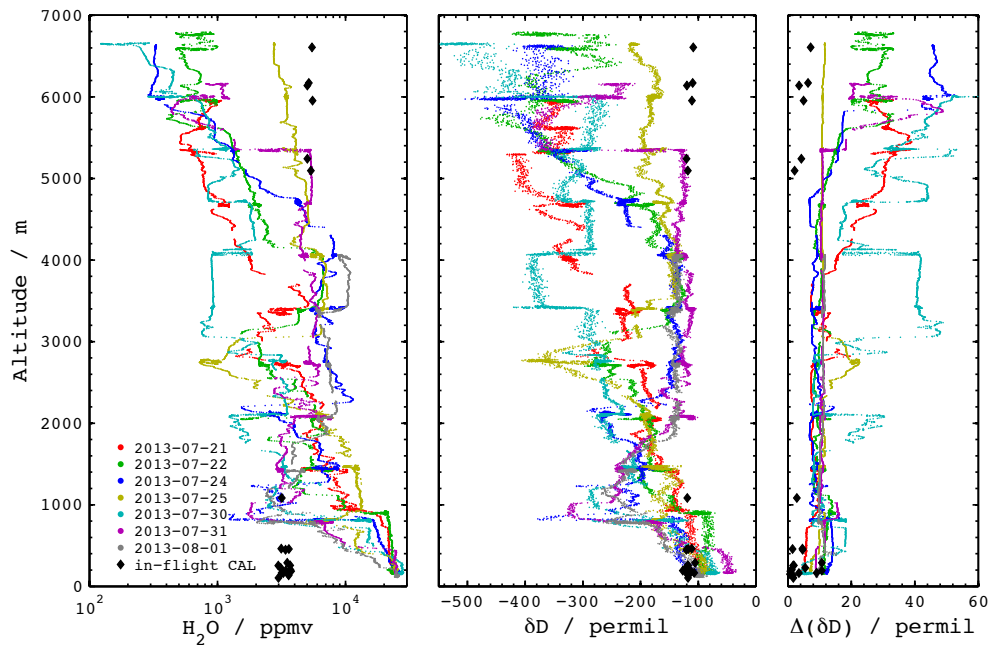


**Figure 9.** Vertical profiles of H<sub>2</sub>O (left),  $\delta D$  (center), and instrumental absolute uncertainty (right) of all flight days evaluated at 1 Hz. For better clarity we show here only data with aircraft descending. Black symbols denote the respective quantities of the inflight calibration-gas measurements.

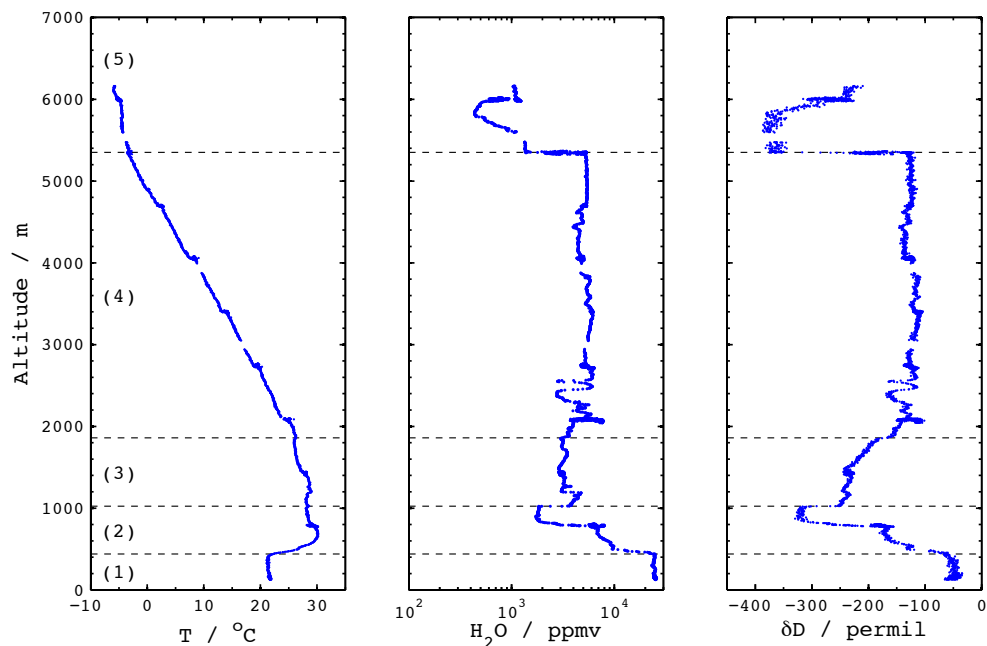


**Figure 10.** Measurements of temperature ( $T$ ), H<sub>2</sub>O mixing ratio, and  $\delta D$  taken with 1 s averaging on 31 July 2013. The profile is divided into five layers for interpretation.

5. At an altitude of around 5350 m we encountered an abrupt decrease in both H<sub>2</sub>O and  $\delta D$  as the aircraft flew at constant altitude in easterly direction. Above we measured the lowest humidity at around 430 ppmv and  $\delta D \approx -370$ ‰.

In order to investigate the processes that may have led to the observed humidity distribution, we depict  $\delta D$  as a function of H<sub>2</sub>O (Fig. 11). By doing so it becomes immediately evident that  $\delta D$  measurements provide additional information, because we observed a rather large range of  $\delta D$

for similar humidity, especially when between around 1000 and 8000 ppmv. We may now be able to identify individual hydration processes by comparing our measurements with model calculations. The Rayleigh model describes an atmosphere in which water vapor condenses at a relative humidity of 100 % and the condensate is immediately removed from the atmosphere by precipitation. The isotopic composition of the condensed phase is defined by the temperature-dependent vapor-pressure isotope fractionation (Dansgaard, 1964). The heavy isotopologue HDO condenses preferentially over H<sub>2</sub><sup>16</sup>O due to its lower vapor pressure. The remaining vapor is becoming more depleted in HDO as the air becomes dryer.

Here we consider ocean water as the major source of atmospheric vapor. Around the Canary Islands, the ocean water has  $\delta D_{ow} \approx +7\text{‰}$  w.r.t. VSMOW (Benetti et al., 2014). The sea surface temperature (SST), which is used to derive the initial isotope fractionation during evaporation, was around 22.5 °C (NOAA\_OI\_SST\_V2 data, <http://www.esrl.noaa.gov/psd/>). Assuming a relative humidity w.r.t. SST of  $RH_{SST} = 80\%$ , the initial vapor has H<sub>2</sub>O  $\approx 23\,000$  ppmv and  $\delta D_{ev} \approx -70\text{‰}$  with respect to the liquid source reservoir. The grey shaded area in Fig. 11 depicts a range of Rayleigh models for  $\delta D_{ow} = 0\text{‰}$  (lower boundary) and  $\delta D_{ow} = +7\text{‰}$  (upper boundary).

First consider the most humid measurements (layer 1) marked with (1) in Fig. 11. These measurements were taken at an altitude of less than 440 m above the ocean, and they are around 20 ‰ above the Rayleigh model. The elevated  $\delta D$  may be due to the evaporation of a fraction of sea spray into the lower atmosphere, a process suggested, e.g., by Benetti et al. (2014).

We note that on this particular day the wind above the ocean was strong, and the lowest atmospheric layer was very hazy. This was confirmed by particle concentration measurements (not shown), which showed elevated concentrations of small particles (size < 3 μm) below 500 m altitude.

If the droplets evaporate (even partially),  $\delta D$  of the vapor becomes less negative (Gat et al., 2003; Benetti et al., 2014). We can estimate the fraction  $F$  of sea spray that evaporated without fractionation and mixed with evaporated ocean water by solving

$$\delta D = F\delta D_{ow} + (1 - F)\delta D_{ev}. \quad (3)$$

Here  $\delta D = -50\text{‰}$  was measured, and  $\delta D_{ow} = +7\text{‰}$  as well as  $\delta D_{ev} = -70\text{‰}$  are assumed. Consequently  $F = 0.26$ , i.e., 26 % of the total water vapor may have originated from the evaporation of sea spray without significant fractionation. Analyzing H<sub>2</sub>O vapor samples for their  $\delta D$ , Gat et al. (2003) concluded that in this particular study up to 50 % of the H<sub>2</sub>O vapor may have originated from evaporated sea spray.

Above this humid layer we observed a very sharp humidity gradient, where the humidity decreased by more than 1 order of magnitude. These data (layer 2) remain close to the theoretical Rayleigh model (blue data in Fig. 11). This suggests

that the dehydration of this air occurred predominantly close to isotopic equilibrium as the air mass was lofted and cooled. These observations were taken in the (locally) warmest layer, where the lowest humidity suggests a temperature of last condensation of around  $-12\text{°C}$  at the sampling pressure. This in turn leads to the conclusion that this air mass must have originated from much higher than the sampling altitude. Descent and adiabatic warming lead to a strong decrease of relative humidity versus ice to  $\sim 8\%$  (not shown), a process termed subsidence drying (Sherwood et al., 2010). The altitude of origin of this air mass was above 5000 m.

At an altitude between 1000 and 1900 m (layer 3), we observed a steady increase of  $\delta D$ , while the humidity remained relatively constant at around 3000 ppmv. This transition is well defined in Fig. 11 and shows a very tightly correlated group of data (medium blue).

In layer 4, extending between around 1900 and 5400 m, we observed a relatively compact distribution of  $\delta D$  and humidity. There,  $\delta D$  is significantly elevated with respect to the Rayleigh model. This suggests that a considerable fraction of the water content is originating from processes other than slow ascent and dehydration of boundary layer air. A model based on the method described by Noone et al. (2011) that describes mixing of moist air typical of the MBL (H<sub>2</sub>O = 22 900 ppmv,  $\delta D = -75.6\text{‰}$ ) and dry air from the upper troposphere (UT; H<sub>2</sub>O = 1100 ppmv,  $\delta D = -385\text{‰}$ ) excellently fits our observations (solid line (4) in Fig. 11).

Layer 4 also showed elevated concentrations of dust (not shown) which originated from the Sahara (see Fig. 8). This suggests that the observed air mass is likely a mixture of MBL air, continental Saharan boundary layer air, and dry air of the UT. The range of humidity and  $\delta D$  suggest that we observed different fractions of moist and dry air. At the top of this layer we observed an abrupt change towards dry UT air with  $\delta D$  close to the Rayleigh model.

Above 5400 m (layer 5) we observed a dryer layer spanning a large range of  $\delta D$  between  $-200\text{‰}$  and  $-380\text{‰}$ . The measurements could be fit to a mixing model line between a low-altitude reservoir of H<sub>2</sub>O = 4900 ppmv and  $\delta D = -133\text{‰}$  and a higher-altitude reservoir with H<sub>2</sub>O = 500 ppmv and  $\delta D = -373\text{‰}$  (solid line (5) in Fig. 11).

## 5 Conclusions

In this paper we present details of an instrument and methods to perform measurements of  $\delta D$ . The instrument and methods were successfully applied in vertical-profile flights during the MUSICA airborne research campaign at the Canary Islands in the summer of 2013 (Schneider et al., 2014). The campaign mainly focused on the validation of remote sensing measurements from ground and space by performing simultaneous in situ measurements. The airborne sampling measurements were performed with the ISOWAT II tunable diode

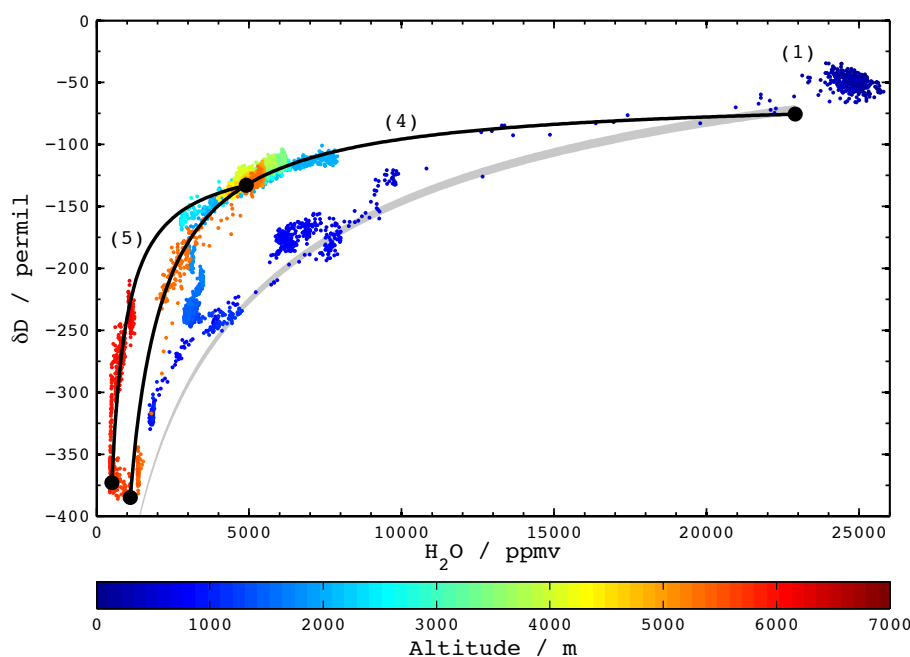


**Figure 11.** Distribution of H<sub>2</sub>O and  $\delta$ D measurements (1 Hz) during the descending branch of the flight on 31 July 2013. The color code represents the sampling altitude. The grey shaded area depicts a range of possible Rayleigh models assuming SST = 22.5 °C and RH = 80 % for ocean water with  $\delta$ D = 0 ‰ (VSMOW, lower boundary) and  $\delta$ D = +7 ‰ (upper boundary). The solid lines represent air mass mixing of (4) MBL and UT air and (5) air at intermediate altitude and UT air (numbers according to levels in Fig. 10).

laser spectrometer. Modifications to ISOWAT (Dyroff et al., 2010) were implemented prior to the campaign aiming to provide measurements with better accuracy and well-defined uncertainty.

During the MUSICA campaign seven flights were performed during which vertical profiles of  $\delta$ D in the troposphere in the subtropical North Atlantic near Tenerife were measured. The profiles were ranging between sea level and around 7 km altitude. The flights were coordinated in time and space with  $\delta$ D remote sensing measurements from ground by the FTIR spectrometer at Izaña, Tenerife, as well as from space by the IASI instruments onboard the MetOp-A and B polar orbiting satellites.

With ISOWAT II we demonstrated  $\delta$ D measurements in situ with a temporal resolution of 1 s. This translated to a horizontal resolution of around 75–95 m and vertical resolution of around 3 m. This allowed resolving even very sharp vertical gradients found both in humidity and  $\delta$ D. A rather extensive calibration protocol allowed determining a robust uncertainty estimate of our  $\delta$ D measurements, i.e., a mandatory requirement for validation measurements. The uncertainty depends on humidity. For most conditions during the campaign the uncertainty was around 10 ‰. Only in the arid upper troposphere was the uncertainty somewhat higher.

Using one flight as an example, five different air mass layers could be identified. Their humidity could be analyzed based on the H<sub>2</sub>O and  $\delta$ D measurements as well as using relatively simple models for dehydration and air mass mix-

ing. Further data analysis is presently being done to better describe both large- and small-scale atmospheric processes based on our measurements.

In a recent paper by Schneider et al. (2014), the ISOWAT II in situ measurements presented here were used for a first validation of space- and ground-based remote sensing measurements of  $\delta$ D. We aim to enlarge the data set for this purpose by performing regular profiling of the troposphere with a new version of ISOWAT onboard the IAGOS-CARIBIC passenger aircraft (Brenninkmeijer et al., 2007).

*Acknowledgements.* We thank Maria Molina Martinez and her colleagues at INTA as well as the pilots for the good organization and realization of the MUSICA aircraft campaign. Part of this study was performed under grant DY 101/1-2 of the DFG SPP 1294. The MUSICA airborne mission was funded in part by the European Research Council under the European Community's Seventh Framework Programme (FP7/2007-2013)/ERC grant agreement no. 256961. We acknowledge support by Deutsche Forschungsgemeinschaft and Open Access Publishing Fund of Karlsruhe Institute of Technology.

The article processing charges for this open-access publication were covered by a Research Centre of the Helmholtz Association.

Edited by: T. F. Hanisco

## References

- Alonso-Pérez, S., Cuevas, E., and Querol, X.: Objective identification of synoptic meteorological patterns favouring African dust intrusions into the marine boundary layer of the subtropical eastern north Atlantic region, *Meteorol. Atmos. Phys.*, 113, 109–124, doi:10.1007/s00703-011-0150-z, 2011.
- Benetti, M., Reverdin, G., Pierre, C., Merlivat, L., Risi, C., Steen-Larsen, H. C., and Vimeux, F.: Deuterium excess in marine water vapor: Dependency on relative humidity and surface wind speed during evaporation, *J. Geophys. Res.-Atmos.*, 119, 584–593, doi:10.1002/2013JD020535, 2014.
- Blumstein, D., Chalou, G., Carlier, T., Buil, C., Hebert, P., Maciaszek, T., Ponce, G., Phulpin, T., Tournier, B., Simeoni, D., Astruc, P., Clauss, A., Kayal, G., and Jegou, R.: IASI instrument: technical overview and measured performances, *Proc. SPIE*, 5543, 196–207, doi:10.1117/12.560907, 2004.
- Boesch, H., Deutscher, N. M., Warneke, T., Byckling, K., Cogan, A. J., Griffith, D. W. T., Notholt, J., Parker, R. J., and Wang, Z.: HDO/H<sub>2</sub>O ratio retrievals from GOSAT, *Atmos. Meas. Tech.*, 6, 599–612, doi:10.5194/amt-6-599-2013, 2013.
- Bolot, M., Legras, B., and Moyer, E. J.: Modelling and interpreting the isotopic composition of water vapour in convective updrafts, *Atmos. Chem. Phys.*, 13, 7903–7935, doi:10.5194/acp-13-7903-2013, 2013.
- Brenninkmeijer, C. A. M., Crutzen, P., Boumard, F., Dauer, T., Dix, B., Ebinghaus, R., Filippi, D., Fischer, H., Franke, H., Frieß, U., Heintzenberg, J., Helleis, F., Hermann, M., Kock, H. H., Koepfel, C., Lelieveld, J., Leuenberger, M., Martinsson, B. G., Miemczyk, S., Moret, H. P., Nguyen, H. N., Nyfeler, P., Oram, D., O'Sullivan, D., Penkett, S., Platt, U., Pupek, M., Ramonet, M., Randa, B., Reichelt, M., Rhee, T. S., Rohwer, J., Rosenfeld, K., Scharffe, D., Schlager, H., Schumann, U., Slemr, F., Sprung, D., Stock, P., Thaler, R., Valentino, F., van Velthoven, P., Waibel, A., Wandel, A., Waschitschek, K., Wiedensohler, A., Xueref-Remy, I., Zahn, A., Zech, U., and Ziereis, H.: Civil Aircraft for the regular investigation of the atmosphere based on an instrumented container: The new CARIBIC system, *Atmos. Chem. Phys.*, 7, 4953–4976, doi:10.5194/acp-7-4953-2007, 2007.
- Burch, D. E., Singleton, E. B., and Williams, D.: Absorption Line Broadening in the Infrared, *Appl. Optics*, 1, 359–363, doi:10.1364/AO.1.000359, 1962.
- Cuevas, E., González, Y., Rodríguez, S., Guerra, J. C., Gómez-Peláez, A. J., Alonso-Pérez, S., Bustos, J., and Milford, C.: Assessment of atmospheric processes driving ozone variations in the subtropical North Atlantic free troposphere, *Atmos. Chem. Phys.*, 13, 1973–1998, doi:10.5194/acp-13-1973-2013, 2013.
- Dansgaard, W.: Stable isotopes in precipitation, *Tellus*, 16, 436–468, 1964.
- Dyroff, C., Fütterer, D., and Zahn, A.: Compact diode-laser spectrometer ISOWAT for highly sensitive airborne measurements of water-isotope ratios, *Appl. Phys. B*, 98, 537–548, doi:10.1007/s00340-009-3775-6, 2010.
- Frankenberg, C., Yoshimura, K., Warneke, T., Aben, I., Butz, A., Deutscher, N., Griffith, D., Hase, F., Notholt, J., Schneider, M., Schrijver, H., and Röckmann, T.: Dynamic Processes Governing Lower-Tropospheric HDO/H<sub>2</sub>O Ratios as Observed from Space and Ground, *Science*, 325, 1374–1377, doi:10.1126/science.1173791, 2009.
- Gat, J. R., Klein, B., Kushnir, Y., Roether, W., Wernli, H., Yam, R., and Shemesh, A.: Isotope composition of air moisture over the Mediterranean Sea: an index of the air–sea interaction pattern, *Tellus B*, 55, 953–965, doi:10.1034/j.1600-0889.2003.00081.x, 2003.
- Herman, R. L., Cherry, J. E., Young, J., Welker, J. M., Noone, D., Kulawik, S. S., and Worden, J.: Aircraft validation of Aura Tropospheric Emission Spectrometer retrievals of HDO/H<sub>2</sub>O, *Atmos. Meas. Tech.*, 7, 3127–3138, doi:10.5194/amt-7-3127-2014, 2014.
- Iannone, R. Q., Kassi, S., Jost, H.-J., Chenevier, M., Romanini, D., Meijer, H. A. J., Dhaniyala, S., Snels, M., and Kerstel, E. R. T.: Development and airborne operation of a compact water isotope ratio infrared spectrometer, *Isot. Environ. Health S.*, 45, 303–320, doi:10.1080/10256010903172715, 2009.
- Jouzel, J. and Merlivat, L.: Deuterium and Oxygen 18 in Precipitation: Modeling of the Isotopic Effects During Snow Formation, *J. Geophys. Res.*, 89, 11749–11757, 1984.
- Klaes, K. D., Cohen, M., Buhler, Y., Schlüssel, P., Munro, R., Engeln, A., Clérigh, E., Bonekamp, H., Ackermann, J., Schmetz, J., and Luntama, J.-P.: An Introduction to the EU-METSAT Polar system, *B. Am. Meteorol. Soc.*, 88, 1085–1096, doi:10.1175/BAMS-88-7-1085, 2007.
- Kuang, Z., Toon, G. C., Wennberg, P. O., and Yung, Y. L.: Measured HDO/H<sub>2</sub>O ratios across the tropical tropopause, *Geophys. Res. Lett.*, 30, 1372, doi:10.1029/2003GL017023, 2003.
- Lacour, J.-L., Risi, C., Clarisse, L., Bony, S., Hurtmans, D., Clerbaux, C., and Coheur, P.-F.: Mid-tropospheric dD observations from IASI/MetOp at high spatial and temporal resolution, *Atmos. Chem. Phys.*, 12, 10817–10832, doi:10.5194/acp-12-10817-2012, 2012.
- Merlivat, L.: Molecular diffusivities of H<sub>2</sub><sup>16</sup>O, HD<sup>16</sup>O, and H<sub>2</sub><sup>18</sup>O in gases, *J. Chem. Phys.*, 69, 2864–2871, 1978.
- Noone, D., Galewsky, J., Sharp, Z. D., Worden, J., Barnes, J., Baer, D., Bailey, A., Brown, D. P., Christensen, L., Crosson, E., Dong, F., Hurley, J. V., Johnson, L. R., Strong, M., Toohey, D., Van Pelt, A., and Wright, J. S.: Properties of air mass mixing and humidity in the subtropics from measurements of the D/H isotope ratio of water vapor at the Mauna Loa Observatory, *J. Geophys. Res.*, 116, doi:10.1029/2011JD015773, 2011.
- Randel, W. J., Moyer, E., Park, M., Jensen, E., Bernath, P., Walker, K., and Boone, C.: Global variations of HDO and HDO/H<sub>2</sub>O ratios in the upper troposphere and lower stratosphere derived from ACE-FTS satellite measurements, *J. Geophys. Res.-Atmos.*, 117, D06303, doi:10.1029/2011JD016632, 2012.
- Risi, C., Bony, S., Vimeux, F., Frankenberg, C., Noone, D., and Worden, J.: Understanding the Sahelian water budget through the isotopic composition of water vapor and precipitation, *J. Geophys. Res.-Atmos.*, 115, D24110, doi:10.1029/2010JD014690, 2010.
- Risi, C., Noone, D., Worden, J., Frankenberg, C., Stiller, G., Kiefer, M., Funke, B., Walker, K., Bernath, P., Schneider, M., Wunch, D., Sherlock, V., Deutscher, N., Griffith, D., Wennberg, P. O., Strong, K., Smale, D., Mahieu, E., Barthlott, S., Hase, F., Garcia, O., Notholt, J., Warneke, T., Toon, G., Sayres, D., Bony, S., Lee, J., Brown, D., Uemura, R., and Sturm, C.: Process-evaluation of tropospheric humidity simulated by general circulation models using water vapor isotopologues: I. Compar-

- ison between models and observations, *J. Geophys. Res.*, 117, D05303, doi:10.1029/2011JD016621, 2012.
- Rodríguez, S., Torres, C., Guerra, J.-C., and Cuevas, E.: Transport pathways of ozone to marine and free-troposphere sites in Tenerife, Canary Islands, *Atmos. Environ.*, 38, 4733–4747, doi:10.1016/j.atmosenv.2004.05.021, 2004.
- Sayres, D. S., Moyer, E. J., Hanisco, T. F., Clair, J. M. S., Keutsch, F. N., O'Brien, A., Allen, N. T., Lapson, L., Demusz, J. N., Rivero, M., Martin, T., Greenberg, M., Tuozzolo, C., Engel, G. S., Kroll, J. H., Paul, J. B., and Anderson, J. G.: A new cavity based absorption instrument for detection of water isotopologues in the upper troposphere and lower stratosphere, *Rev. Sci. Instrum.*, 80, 044102, doi:10.1063/1.3117349, 2009.
- Schneider, M. and Hase, F.: Optimal estimation of tropospheric H<sub>2</sub>O and δD with IASI/METOP, *Atmos. Chem. Phys.*, 11, 11207–11220, doi:10.5194/acp-11-11207-2011, 2011.
- Schneider, M., Hase, F., and Blumenstock, T.: Ground-based remote sensing of HDO/H<sub>2</sub>O ratio profiles: introduction and validation of an innovative retrieval approach, *Atmos. Chem. Phys.*, 6, 4705–4722, doi:10.5194/acp-6-4705-2006, 2006.
- Schneider, M., Barthlott, S., Hase, F., González, Y., Yoshimura, K., García, O. E., Sepúlveda, E., Gomez-Pelaez, A., Gisi, M., Kohlhepp, R., Dohe, S., Blumenstock, T., Wiegeler, A., Christner, E., Strong, K., Weaver, D., Palm, M., Deutscher, N. M., Warneke, T., Notholt, J., Lejeune, B., Demoulin, P., Jones, N., Griffith, D. W. T., Smale, D., and Robinson, J.: Ground-based remote sensing of tropospheric water vapour isotopologues within the project MUSICA, *Atmos. Meas. Tech.*, 5, 3007–3027, doi:10.5194/amt-5-3007-2012, 2012.
- Schneider, M., González, Y., Dyroff, C., Christner, E., Wiegeler, A., Barthlott, S., García, O. E., Sepúlveda, E., Hase, F., Andrey, J., Blumenstock, T., Guirado, C., Ramos, R., and Rodríguez, S.: Empirical validation and proof of added value of MUSICA's tropospheric dD remote sensing products, *Atmos. Meas. Tech.*, 8, 483–503, doi:10.5194/amt-8-483-2015, 2015.
- Sherwood, S. C., Roca, R., Weckwerth, T. M., and Andronova, N. G.: Tropospheric water vapor, convection, and climate, *Rev. Geophys.*, 48, RG2001, doi:10.1029/2009RG000301, 2010.
- Sodemann, H., Aemisegger, F., Pfahl, S., Corsmeier, U., Wieser, A., Bitter, M., Feuerle, T., Hankers, R., Schulz, H., Hsiao, G., and Wernli, H.: High-resolution vertical profiles of stable water isotopes from airborne measurements in the western Mediterranean during HyMeX in October 2012, *Geoph. Res. Abs.*, 15, 12674, available at: <http://meetingorganizer.copernicus.org/EGU2013/EGU2013-12674.pdf> (last access: 19 March 2014), 2013.
- Webster, C. R. and Heymsfield, A. J.: Water Isotope Ratios D/H, <sup>18</sup>O/<sup>16</sup>O, <sup>17</sup>O/<sup>16</sup>O in and out of Clouds Map Dehydration Pathways, *Science*, 302, 1742–1745, 2003.
- Wiegeler, A., Schneider, M., Hase, F., Barthlott, S., García, O. E., Sepúlveda, E., González, Y., Blumenstock, T., Raffalski, U., Gisi, M., and Kohlhepp, R.: The MUSICA MetOp/IASI H<sub>2</sub>O and dD products: characterisation and long-term comparison to NDACC/FTIR data, *Atmos. Meas. Tech.*, 7, 2719–2732, doi:10.5194/amt-7-2719-2014, 2014.
- Worden, J., Bowman, K., Noone, D., Beer, R., Clough, S., Eldering, A., Fisher, B., Goldman, A., Gunson, M., Herman, R., Kulawik, S. S., Lampel, M., Luo, M., Osterman, G., Rinsland, C., Rodgers, C., Sander, S., Shephard, M., and Worden, H.: Tropospheric Emission Spectrometer observations of the tropospheric HDO/H<sub>2</sub>O ratio: Estimation approach and characterization, *J. Geophys. Res.*, 111, D16309, doi:10.1029/2005JD006606, 2006.
- Worden, J., Noone, D., Galewsky, J., Bailey, A., Bowman, K., Brown, D., Hurley, J., Kulawik, S., Lee, J., and Strong, M.: Estimate of bias in Aura TES HDO/H<sub>2</sub>O profiles from comparison of TES and in situ HDO/H<sub>2</sub>O measurements at the Mauna Loa observatory, *Atmos. Chem. Phys.*, 11, 4491–4503, doi:10.5194/acp-11-4491-2011, 2011.
- Zakharov, V. I., Imasu, R., Gribanov, K. G., Hoffmann, G., and Jouzel, J.: Latitudinal distribution of the deuterium to hydrogen ratio in the atmospheric water vapor retrieved from IMG/ADEOS data, *Geophys. Res. Lett.*, 31, L12104, doi:10.1029/2004GL019433, 2004.